

# Unveiling the $S=3/2$ Kitaev Honeycomb Spin Liquids

Hui-Ke Jin,<sup>1</sup> W. M. H. Natori,<sup>2,3</sup> F. Pollmann,<sup>4,5</sup> and J. Knolle<sup>1,5,3</sup>

<sup>1</sup>Department of Physics TQM, Technische Universität München, James-Frank-Straße 1, D-85748 Garching, Germany

<sup>2</sup>Institute Laue-Langevin, BP 156, 41 Avenue des Martyrs, 38042 Grenoble Cedex 9, France

<sup>3</sup>Blackett Laboratory, Imperial College London, London SW7 2AZ, United Kingdom

<sup>4</sup>Department of Physics CMT, Technische Universität München, James-Frank-Straße 1, D-85748 Garching, Germany

<sup>5</sup>Munich Center for Quantum Science and Technology (MCQST), 80799 Munich, Germany

(Dated: July 29, 2021)

The  $S=3/2$  Kitaev honeycomb model (KHM) has defied an analytical as well as numerical understanding because it is not exactly soluble like its  $S=1/2$  brethren and in contrast to other spin- $S$  Kitaev models numerical methods are plagued by a massive pile up of low energy states. Here, we uncover the phase diagram of the  $S=3/2$  KHM and find gapped and gapless quantum spin liquids (QSLs) generally coexisting with spin quadrupolar orders. Employing an  $SO(6)$  Majorana fermion representation of spin- $3/2$ 's, we find an exact representation of the conserved plaquette fluxes in terms of static  $Z_2$  gauge fields akin to the  $S=1/2$  KHM which enables us to treat the remaining interacting matter fermion sector in a parton mean-field theory. The latter provides an explanation for the extensive near degeneracy of low energy states in the gapless phase via the appearance of almost flat Majorana bands close to zero energy. Our parton description is in remarkable quantitative agreement with numerical simulations using the density matrix renormalization group method, and is furthermore corroborated by the addition of a single ion anisotropy which continuously connects the gapless Dirac QSL of our model with that of the  $S=1/2$  KHM. We discuss the implications of our findings for materials realization of higher  $S=3/2$  KHMs and the stability of the QSL phase with respect to additional interactions.

*Introduction.* The search for QSLs has been at the forefront of condensed matter physics for many decades because they represent novel quantum phases of matter beyond the Landau paradigm of symmetry breaking — instead they are characterized by fractionalized excitations and non-local quantum entanglement [1–4]. A paradigmatic example of a two-dimensional (2D) QSL is the seminal Kitaev honeycomb model (KHM) [5], which was initially derived to illustrate the basic ideas of topological quantum computation [6]. Remarkably, the model has an exact solution which shows that its excitations are free Majorana fermions with a Dirac dispersion and gapped conserved plaquette fluxes which couple to the Majoranas via a *static*  $Z_2$  gauge field. In the context of frustrated magnetism research, the KHM provided a first rigorous example how a QSL with fractionalized excitations and emergent gauge fields can emerge in a microscopic 2D spin model with only nearest neighbor interactions.

In the last years, the KHM has transformed from a theoretical toy model to one of experimental relevance because a flurry of spin-orbit-coupled  $4d$  and  $5d$  transition metal compounds [7–12] have been proposed as candidates for realizing its bond-anisotropic Ising interactions. Remarkably, experiments have also observed signatures of the proximate Kitaev spin liquid (KSL) in several materials with effective spin  $1/2$  moments, such as  $\alpha$ - $\text{RuCl}_3$  [13–18] and  $(\text{Na}_{1-x}\text{Li}_x)_2\text{IrO}_3$  [19, 20], despite the residual zigzag ordered state which appears at low temperature [21, 22] because of additional interactions, e.g. an off-diagonal symmetric  $\Gamma$  exchange [13]. However, the exchange frustration of the KHM is not restricted to spin  $1/2$  and recently some promising realizations of higher-spin Kitaev materials have been proposed based upon  $3d$  orbitals [23–25], in which the QSL-disrupting non-Kitaev exchanges might be reduced [26–28]. In particular, a microscopic derivation of the  $S=3/2$  KHM model with an extra sin-

gle ion anisotropy (SIA) has been established for the quasi 2D systems  $\text{CrI}_3$  and  $\text{CrGeTe}_3$  [24, 25].

After the original proposal of the  $S=1/2$  KHM [5], much effort has been devoted to investigating the KHM models for  $S>1/2$ , which have not found an exact solution [29–36]. Nevertheless, Baskaran and collaborators [30] showed early on that a generic spin- $S$  KHM still has conserved  $Z_2$  fluxes for each elementary hexagon and suggested via a semiclassical analysis that the ground state of the KHM for all values of  $S$  exhibits a homogeneous flux configuration in which all values of  $Z_2$  fluxes are  $+1$  [30]. Subsequently, it has been proposed that the ground states of the  $S>3/2$  KHMs are  $Z_2$  QSLs described by an effective toric code on a honeycomb superlattice, but the employed semi-classical analysis breaks down precisely at  $S=3/2$  [34]. The  $S=1$  KHM is amenable to numerical investigations and studies using exact diagonalization [33] and density matrix renormalization group (DMRG) [35] methods point to a gapless QSL ground state, whereas a tensor network approach proposes a gapped QSL for the isotropic model [36]. Overall, the  $S=3/2$  KHM seems to be the least understood of all Kitaev models — the conserved plaquette fluxes alone do not help to gain an analytical understanding and a high density of low energy excitations lead to strong finite size effects for numerical investigations.

Here, we report new exact properties of the  $S=3/2$  KHM and provide a systematic understanding of its ground-state phase diagram and excitations. We introduce an  $SO(6)$  Majorana representation for the spin- $3/2$ 's which permits an exact mapping of the spin model to one of fermions coupled to a *static*  $Z_2$  gauge field. The latter determines the conserved plaquette flux just like in the original  $S=1/2$  KHM. Within a given gauge field configuration, the Hamiltonian still contains quartic and even sextic fermion interaction terms but we construct a parton mean-field theory which turns out to be even

quantitatively reliable. It allows us to map out the phase diagram consisting of two gapless Dirac and one gapped QSLs. Our theory is furthermore corroborated by the addition of an extra SIA to the S=3/2 KHM, which still preserves the conservation of the  $Z_2$  fluxes. In the limit of an extremely large SIA, we find an exact solution of an effective S=1/2 KSL, which is continuously connected to one of the two gapless phases of the pure S=3/2 KHM. Finally, we investigate the model using the DMRG method [37, 38] and find the numerical results to be in quantitative agreement with the predictions from our parton mean-field theory.

*Model Hamiltonian.* The Hamiltonian of the S=3/2 KHM reads

$$\mathcal{H} = \sum_{\langle ij \rangle_a} J_a S_i^a S_j^a, \quad (1)$$

where  $S_i^a$  ( $a = x, y, z$ ) are three components of an S=3/2 spin at site  $i$  and  $\langle ij \rangle_a$  denotes the nearest neighbor (NN) bonds of  $a$ -type S=3/2 Ising interactions (see Fig. 1). Here we only consider the antiferromagnetic couplings of  $J_a > 0$  since the signs of  $J_a$  do not change the main results of this work. There exist commuting plaquette operators  $W_p$  for each hexagon  $p$  (see Fig. 1) as  $W_p \equiv -e^{i\pi(S_1^x+S_2^y+S_3^z+S_4^x+S_5^y+S_6^z)}$  [30]. By noticing that  $[W_p, \mathcal{H}] = 0$ , the total Hilbert space of Hamiltonian (1) can be divided into orthogonal sectors characterized by flux configurations  $\{w_p = \pm 1\}$ , where  $w_p$  is the eigenvalue of  $W_p$ .

The microscopic derivation of the S=3/2 KHM introduced in Ref. [25] suggests that it is usually accompanied by an extra SIA term of the form  $(\sum_a S_i^a)^2$ . However, such a term does not commute with the local plaquette operators and breaks the corresponding conservation law. Instead, we consider the KHM with a simplified SIA term, which is described by the Hamiltonian

$$\mathcal{H}_{Dz} = \mathcal{H} + D_z \sum_i (S_i^z)^2, \quad D_z > 0. \quad (2)$$

Note that the local plaquette operators  $W_p$  do commute with this type of SIA. Since the local S=3/2 states of  $|S_i^z = \pm \frac{3}{2}\rangle$  ( $|S_i^z = \pm \frac{1}{2}\rangle$ ) will be energetically favored when  $J_z$  ( $D_z$ ) dominates, we expect that the competition of  $J_z$  and  $D_z$  will lead to a rich phase diagram. Moreover, below we will show that an effective S=1/2 KSL will emerge in the limit  $D_z \rightarrow \infty$ .

*SO(6) Majorana representation.* The largest symmetry allowed for spins S=3/2 is  $SU(4) \simeq SO(6)$ , thus, one can construct an SO(6) Majorana representation for spin-3/2's [39–52]. We introduce three gauge Majorana fermions  $\eta_i^a$  and three itinerant Majorana fermions  $\theta_i^a$  ( $a = x, y, z$ ), to obtain  $S_i^a = \frac{i}{4} \epsilon_{abc} \eta_i^b \eta_i^c - \frac{i}{2} \eta_i^a \tilde{\theta}_i^a$ , where  $\tilde{\theta}_i^{x(y)} = \theta_i^x - (+) \sqrt{3} \theta_i^y$ ,  $\tilde{\theta}_i^z = -2\theta_i^z$ , and  $\epsilon_{abc}$  is the Levi-Civita tensor (the summation over repeated indices is assumed throughout this work). This parton representation doubly enlarges the Hilbert space and the physical Hilbert space of spin-3/2's can be restored by imposing a local constraint of  $D_i = i\eta_i^x \eta_i^y \eta_i^z \theta_i^x \theta_i^y \theta_i^z = 1$ . By using the constraint, we can obtain  $i\eta_i^b \eta_i^c = \epsilon_{abc} \theta_i^a \theta_i^x \theta_i^y \theta_i^z$  and rewrite the

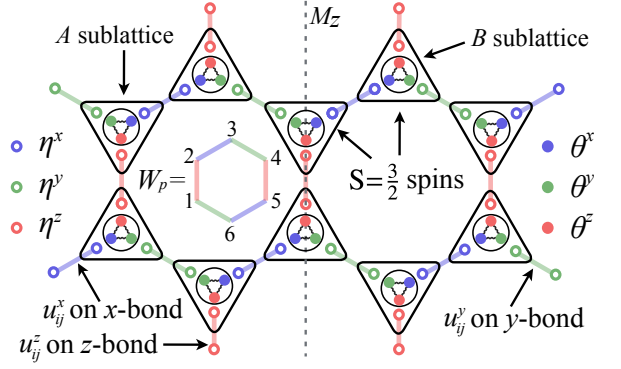


FIG. 1. Graphic representation of the S=3/2 KHM (4) and the SO(6) Majorana representation. Down and up triangles stand for S=3/2 spins on A and B sublattices, respectively. Each spin is represented by SO(6) Majoranas, e.g., three gauge Majoranas  $\eta^{x,y,z}$  (circles) and three itinerant Majoranas  $\theta^{x,y,z}$  (dots). The blue, green, and red bold lines denote the *static*  $Z_2$  gauge fields  $u^x$ ,  $u^y$ , and  $u^z$  for  $x$ -,  $y$ -, and  $z$ -bond Ising interactions, respectively. The plaquette operator  $W_p \equiv -e^{i\pi(S_1^x+S_2^y+S_3^z+S_4^x+S_5^y+S_6^z)}$  can be expressed as the product of  $Z_2$  gauge fields around a hexagon  $p$ . The gray dashed line stands for the mirror symmetry  $M_z$  with  $J_x = J_y$ .

three spin operators as

$$S^a = \frac{i}{2} \eta_i^a (\theta_i^{xyz} - \tilde{\theta}_i^a), \quad (a = x, y, z), \quad (3)$$

where  $\theta_i^{xyz} = -i\theta_i^x \theta_i^y \theta_i^z$ .

By combining Eq. (3) with  $(S_i^z)^2 = -i\theta_i^x \theta_i^y$  (a constant is omitted),  $\mathcal{H}_{Dz}$  in Eq. (2) becomes an effective Hamiltonian for Majorana partons

$$H_{Dz} = -\frac{i}{4} \sum_{\langle ij \rangle_a} J_a u_{ij}^a (\theta_i^{xyz} - \tilde{\theta}_i^a) (\theta_j^{xyz} - \tilde{\theta}_j^a) - iD_z \sum_i \theta_i^x \theta_i^y, \quad (4)$$

where  $u_{ij}^a = i\eta_i^a \eta_j^a$  and we have taken the convention that  $i(j) \in A(B)$  sublattice for NN bond  $\langle ij \rangle_a$ .

One can now verify that  $[u_{ij}^a, u_{kl}^b] = 0$  for all different bonds and  $[u_{ij}^a, H_{Dz}] = 0$ . Therefore, the link variables  $u_{ij}^a$  with eigenvalues  $\pm 1$  is a *static*  $Z_2$  gauge field! Similar to the S=1/2 KHM, the plaquette operator  $W_p$  is exactly mapped to a product of  $u_{ij}^a$  around hexagon  $p$ , e.g.,  $W_p = u_{12}^z u_{32}^x u_{34}^y u_{54}^z u_{56}^x u_{16}^y$  as shown in Fig. 1. When the  $Z_2$  gauge field configuration (denoted by  $\{u\}$ ) is fixed, the corresponding flux configuration is also fixed, which drastically simplifies the complexity of the problem to a Hamiltonian only depending on the itinerant Majoranas  $\theta_i^a$ .

*Mean-field theory.* The effective Hamiltonian (4) can be divided into two parts. One is a quadratic Hamiltonian  $H^{(2)}(\{u\}) \equiv \frac{i}{4} \sum_{\langle ij \rangle_a} J_a u_{ij}^a \tilde{\theta}_i^a \tilde{\theta}_j^a - iD_z \sum_i \theta_i^x \theta_i^y$ , and the other is an interacting Hamiltonian consisting of quartic and sextic terms, which we treat within a mean-field analysis. In our decoupling scheme, the mean-field Hamiltonian can be written in a com-

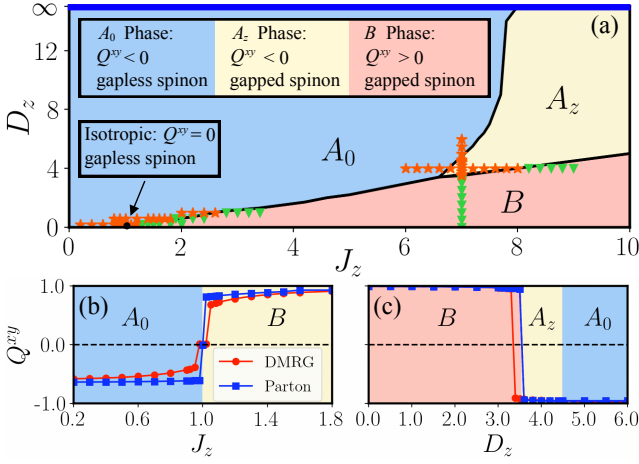


FIG. 2. (a) The mean-field phase diagram of Hamiltonian (5) in the zero-flux sector. The  $A_0$  phase is a Dirac QSL with spin quadrupolar order  $Q^{xy} < 0$ . In the  $A_z$  ( $B$ ) phase, the spinon excitations are gapped with  $Q^{xy} < 0$  ( $Q^{xy} > 0$ ). At the isotropic point, the ground state is a QSL with  $Q^{xy} = 0$ . The bold blue line at  $D_z = \infty$  with  $J_z < 8$  ( $J_z > 8$ ) represents the effective gapless (gapped)  $S=1/2$  KSL. The gapless phases in  $S=3/2$  and  $S=1/2$  KHM can continuously connect to each other through the  $A_0$  phase without energy gap opening. The orange stars (green triangles) represent the ground states obtained by DMRG on a  $3 \times 4$  torus with zero-flux (disordered-flux) configurations. (b, c) The values of  $Q^{xy}$  as a function of  $J_z$  with  $D_z = 0$  (b) and  $D_z$  with  $J_z = 7$  (c). The computations of DMRG and parton mean-field theory are performed on a  $3 \times 4$  torus.

pact form as

$$\begin{aligned}
 H_{\text{MF}}(\{u\}) = & H^{(2)}(\{u\}) + \sum_{\langle ij \rangle_a} \frac{iJ_a u_{ij}^a}{4} \left\{ \frac{\epsilon_{opq} \epsilon_{rst}}{4} \langle \theta_i^o \theta_j^p \theta_j^r \theta_i^s \rangle \theta_i^q \theta_j^t \right. \\
 & + \frac{\epsilon_{lmn}}{2} \left( \theta_i^m \theta_j^n \langle \theta_i^l \theta_j^x \theta_j^y \theta_i^z \rangle - \theta_j^m \theta_i^n \langle \theta_j^l \theta_i^x \theta_i^y \theta_j^z \rangle \right) \\
 & \left. + \frac{\epsilon_{uvw}}{2} \left[ \left( Q_i^{uv} \theta_i^w \tilde{\theta}_j^a - \Delta_{ij}^{w\tilde{a}} \theta_i^u \theta_j^v - Q_i^{uv} \Delta_{ij}^{w\tilde{a}} \right) - (i \leftrightarrow j) \right] \right\}, \quad (5)
 \end{aligned}$$

with the on-site parameters  $Q_i^{ab} \equiv -\langle i\theta_i^a \theta_i^b \rangle$  ( $a \neq b$ ) and bond parameters defined as  $\Delta_{ij}^{ab} \equiv \langle i\theta_i^a \theta_j^b \rangle$  ( $\Delta_{ij}^{\tilde{a}\tilde{b}} \equiv \langle i\theta_i^a \tilde{\theta}_j^b \rangle$ ). In accordance with Wick's theorem, the average of quartic terms can be decoupled as  $\langle \theta_i^o \theta_j^p \theta_j^r \theta_i^s \rangle = -Q_i^{op} Q_j^{rs} + \Delta_{ij}^{or} \Delta_{ij}^{ps} - \Delta_{ij}^{os} \Delta_{ij}^{pr}$  and  $\langle \theta_i^l \theta_j^x \theta_j^y \theta_i^z \rangle = \Delta_{ij}^{lx} Q_j^{yz} + \Delta_{ij}^{ly} Q_j^{zx} + \Delta_{ij}^{lz} Q_j^{xy}$ . Eventually,  $H_{\text{MF}}$  is parameterized by the mean-field parameters  $Q$  and  $\Delta$ , which we determine self-consistently [53]. For simplicity, we focus on the case of  $J_x = J_y$  with a mirror symmetry  $M_z$  across the  $z$ -bonds (see Fig. 1) which leads to a vanishing of the parameters  $Q^{yz}, Q^{zx} = 0$ . The only nonzero on-site parameter is  $Q^{xy} \equiv -\langle i\theta_i^x \theta_i^y \rangle = \langle (S^z)^2 \rangle$  which is a spin quadrupolar component characterizing the mean-field ground states of  $H_{\text{MF}}(\{u\})$ .

Following the proposal of Ref. [30] that for generic spin- $S$  KHM the ground-state always exhibits a zero-flux configuration with all  $\{w_p\} = 1$ , we will mainly focus on the zero-flux sector and fix  $\{u\} = 1$  for studying the spinon excitations of  $H_{\text{MF}}$ . It is worth noting that the quadratic Hamiltonian  $H^{(2)}(\{u\})$  alone always energetically favors a zero-flux state.

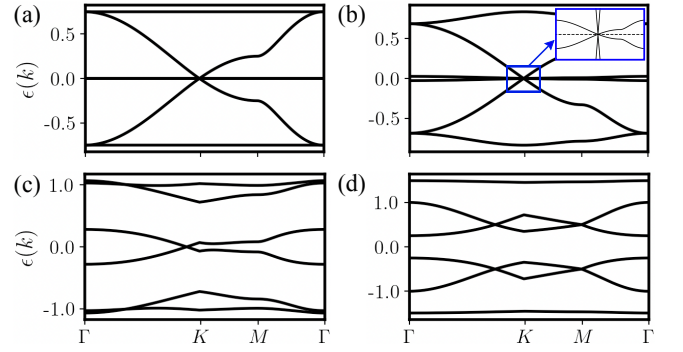


FIG. 3. (a) Spinon band structure of the quadratic Hamiltonian  $H^{(2)}$  at the isotropic point  $J_z = 1$  and  $D_z = 0$ . (b-d) Spinon band structures of the mean-field Hamiltonian  $H_{\text{MF}}$  with (b)  $J_z = 1$  and  $D_z = 0$ , (c)  $J_z = 1.2$  and  $D_z = 0.4$ , and (d)  $J_z = 1.4$  and  $D_z = 0$ . Here  $J_x = J_y = 1$ , and a zero-flux configuration of  $\{u\} = 1$  is used. The inset in (b) shows the zoom-in around the K point.

The Hamiltonian  $H_{\text{MF}}(\{u\} = 1)$  displays four phases which are characterized by their distinct spinon excitations and the quadrupolar order parameter  $Q^{xy}$ , as shown in Fig. 2(a). (i) At the isotropic point of  $J_z = 1$  and  $D_z = 0$ , the ground state is a Dirac QSL with  $Q^{xy} = 0$ . We find that the spinon band structure of  $H_{\text{MF}}(\{u\} = 1)$  at the isotropic point is almost the same as that of the quadratic Hamiltonian  $H^{(2)}(\{u\} = 1)$ , except that the exact flat bands populated by  $\theta^y$  in Fig. 3(a) acquire a very narrow dispersion as shown in Fig. 3(b). Consequently, in this phase  $H_{\text{MF}}(\{u\} = 1)$  has a Dirac point at the K-point, around which there exist two gapless spinon bands crossing linearly at zero energy but one of whose velocity is close to zero. (ii) In the  $A_0$  phase, the ground state is a Dirac QSL coexisting with the spin quadrupolar order parameter  $Q^{xy} < 0$ . Notice that as a consequence of a nonzero  $Q^{xy} < 0$ , only one branch of gapless spin excitations remains around the Dirac point, as shown in Fig. 3(c). (iii) In the  $A_z$  phase, the effect of  $D_z$  remains, but a relatively large anisotropy of  $J_z$  gaps out all spinon excitations and the ground state is a gapped QSL coexisting with a spin quadrupolar order of  $Q^{xy} < 0$ . (iv) In the  $B$  phase, the dominant  $J_z$  leads to a positive  $Q^{xy} > 0$  and all spinon excitations are gapped. The typical spinon band structure for the  $B$  phase is plotted in Fig. 3(d). We conclude that the transition between the  $B$  phase and the  $A_0$  ( $A_z$ ) phase is of first-order since  $Q^{xy}$  shows a discontinuous bump at the phase boundary in Fig. 2(b) and (c).

*Effective  $S=1/2$  KSL.* A key advantage of using the SIA along one of the spin directions, see Eq. (2), is that the Hamiltonian Eq. (4) can be solved exactly for  $D_z \rightarrow \infty$ . In this limit, the high energy local states of  $|S_i^z = \pm \frac{3}{2}\rangle$  are removed and the ground-state subspace of the Hamiltonian in Eq. (2) is spanned by the local states of  $|S_i^z = \pm 1/2\rangle$  only. Within the framework of the  $\text{SO}(6)$  Majorana representation, the itinerant Majoranas  $\theta_i^x$  and  $\theta_i^y$  are paired up subjected to the constraint of  $i\theta_i^x \theta_i^y = 1$  ( $Q^{xy} = -1$ ). We can then project the three  $S=3/2$  spin operators in Eq. (3) onto the subspace of  $i\theta_i^x \theta_i^y = 1$  and



re-expresses them as

$$S_i^z \simeq \frac{i}{2} \eta_i^z \theta_i^z, \quad S_i^{x(y)} \simeq i \eta_i^{x(y)} \theta_i^z. \quad (6)$$

Obviously, Eq. (6) is equivalent to Kitaev's original four-Majorana representation [5]. Notice that the terms corresponding to the high energy excitations, like  $\eta_i^{x(y)} \theta_i^x$ , have been omitted in Eq. (6). It is remarkable that an effective  $S=1/2$  KHM with a renormalized coupling constant  $J_z \rightarrow J_z/4$  emerges in such an  $S=3/2$  Hamiltonian, Eq. (4), with  $D_z \rightarrow \infty$ , in which we can obtain an effective gapless (gapped) KSL for  $J_z < (>) 8$ . This connection gives additional support to the assumption of a zero flux background state and our mean-field treatment, which is known to exactly capture the phase diagram and nature of excitations of the  $S=1/2$  KHM [54, 55]. Indeed, we find that the gapless KSL of the emergent  $S=1/2$  KHM is continuously connected to the gapless phase of the pure  $S=3/2$  KHM without opening a spinon gap throughout the gapless  $A_0$  phase as shown in the phase diagram in Fig. 2(a).

*DMRG study.* In order to examine the reliability of our parton mean-field theory, we employ state-of-the-art DMRG simulations [37, 38] to study the ground state of Eq. (2). DMRG is a very powerful numerical approach for studying strongly-correlated systems in one dimension. To perform DMRG calculations on a 2D honeycomb lattice of  $L_1 \times L_2$  unit cells, we consider a cylindrical geometry for which the periodic boundary condition (PBC) is imposed along the shorter direction (e.g., the circumference,  $L_1$ ), while the longer (e.g., the length,  $L_2$ ) is left open. Moreover, we also adopt small tori with PBCs along both directions to strictly preserve the  $A/B$  sublattice and translational symmetries. The DMRG simulations are performed on a  $3 \times 4$  torus as well as a  $4 \times 8$  cylinder ( $L_1 = 4$ ). The bond dimension of DMRG is kept as large as  $\chi = 4000$ , resulting in a typical truncation error of  $\epsilon \simeq 10^{-6}$  ( $\epsilon \simeq 10^{-4}$  close to the isotropic point  $J_z = 1$  and  $D_z = 0$ ). In general, we encounter significant finite size effects in our numerical studies in contrast to checks on the  $S=1/2$  and 1 KHMs.

Since Lieb's theorem [56] may not be applicable for the interacting Hamiltonian Eq. (4), we examine the the zero-flux ground state configuration, which is a pivotal assumption in our mean-field theory. We find that the ground states in our DMRG simulations always exhibit a zero-flux configuration in the  $A_0$  and  $A_z$  phases for both torus and cylindrical geometries. In contrast, for the  $B$  phase, DMRG does not converge to a unique ground state flux configuration but instead leads to a disordered-flux ground state in which the measured flux for each plaquette is neither 1 nor  $-1$ . The data points for different DMRG-obtained ground-state flux configurations are shown in Fig. 2(a).

The disordered-flux ground states obtained by DMRG indicate an extremely small flux gap above the zero-flux state in the  $B$  phase. The flux gap above the zero-flux state can also be evaluated within our mean-field theory in the  $B$  phase. To connect to our DMRG simulations, we have performed the

mean-field calculations on the same  $3 \times 4$  torus. We find that the energy of a pair of neighboring fluxes is  $E_{2\text{fluxes}} \simeq 10^{-6}$  for  $J_z = 1.2$  and  $D_z = 0$ , which is as small as the corresponding DMRG truncation error  $\epsilon \simeq 10^{-6}$ . The flux gap  $E_{2\text{fluxes}}$  rapidly decreases as the anisotropy  $J_z$  increases. This extremely small flux gap explains why DMRG fails to capture the conserved  $Z_2$  fluxes in the  $B$  phase.

Next, we investigate the local spin quadrupolar order  $Q_i^{xy}$  using DMRG and we find that the  $Q_i^{xy}$  are spatially uniform (on the torus and in the bulk of cylinders) as assumed in our parton description. A remarkable observation is that, if we ignore small discrepancies near the phase boundaries, the values of the DMRG-obtained  $Q^{xy}$  are even in quantitative agreement with those given by the parton mean-field theory within the zero-flux sector, as shown in Fig. 2(b) and (c). For the purpose of comparison, we have chosen the same lattice geometry, e.g., a  $3 \times 4$  torus, to calculate the mean-field and DMRG values of  $Q^{xy}$ . The difference between the mean-field  $Q^{xy}$  for a  $3 \times 4$  torus and its extrapolation to an infinite lattice is of the magnitude of  $10^{-2}$  (except near the phase boundaries), thus finite-size effect for the quadrupolar order are small. This remarkable quantitative agreement demonstrates that our SO(6) Majorana parton mean-field theory provides a compelling scenario for describing the  $S=3/2$  KHM. For example, we can now understand why the  $S=3/2$  KHM at the isotropic point is so challenging for numerical methods, e.g. the extreme system size dependence encountered in our DMRG simulations, because the almost flat Majorana bands, see Fig. 3(b), lead to a large pile up of close to zero energy states.

*Discussion and Outlook.* In summary, we have studied the ground state phase diagram and excitations of the  $S=3/2$  KHM with an additional SIA using a parton theory based on the SO(6) Majorana representation of spin= $3/2$ 's and supported by DMRG simulations. We have shown that the conserved flux operator for each honeycomb plaquette can be represented exactly via a static  $Z_2$  gauge field similar to the well known  $S=1/2$  KHM, which is key for identifying the correct mean-field decoupling of the parton description. Large-scale DMRG calculations are shown to agree with our self-consistent mean-field theory qualitatively and even quantitatively. We uncover a rich phase diagram characterized by distinct Majorana fermion excitations and different phases with spin quadrupolar order  $Q^{xy} = \langle (S^z)^2 \rangle$ : (i) a gapless Dirac QSL with  $Q^{xy} = 0$  and an additional almost flat Majorana band close to zero energy at the isotropic point ( $J_z = 1, D_z = 0$ ); (ii) a gapless Dirac QSL with  $Q^{xy} < 0$  in the  $A_0$  phase; (iii) a gapped QSL with  $Q^{xy} < 0$  in the  $A_z$  phase; and (iv) a gapped QSL with  $Q^{xy} > 0$  in the  $B$  phase. In the limit of a dominating SIA, the low energy sector of the  $S=3/2$ s reduces to effective  $S=1/2$ s which allows us to continuously connect the gapless  $A_0$  phase of the pure  $S=3/2$  KHM to that of the well known Dirac QSL of the  $S=1/2$  KHM. In the  $B$  phase, we found that DMRG fails to capture the conservation of  $Z_2$  fluxes because of an extremely small flux gap above the zero-flux ground state, which is again accounted for in our mean-field theory.

We argue that our SO(6) Majorana parton theory efficiently

describes the different QSLs of the  $S=3/2$  KHM, which also provides a compelling scenario for explaining the difficulties encountered in the numerical studies. Hence, it will provide an excellent starting point for studying the robustness of the QSL regimes with respect to additional terms in the Hamiltonian, for example different exchange interactions and the SIA relevant for microscopic realizations of the  $S=3/2$  KHM [25]. The connection to the  $S=1/2$  KHM indicates that in particular the ferromagnetic QSLs will be very fragile and, in general, the formation of conventional magnetic order will be further facilitated because of flux-fermion boundstate formation involving the almost flat Majorana bands. In that context, the quality of our parton mean-field states can be further improved by efficient tensor network representation with Gutzwiller projection [57–59] or by including different flux sectors in the variational ansatz [60].

In the future, it will be very worthwhile to study the effect of applying a magnetic field and the ensuing QSL phases of the  $S=3/2$  KHM. Similarly, it would be desirable to generalize our Majorana parton construction to higher-spin systems whose dimension of local Hilbert space is  $2^n$  (with  $n$  integer), *i.e.* the  $S=7/2$  KHM could possibly have a similar exact static  $Z_2$  gauge field permitting an efficient description via an eight Majorana representation for spin- $7/2$ 's.

*Acknowledgement.* F. P. acknowledges the support of the Deutsche Forschungsgemeinschaft (DFG, German Research Foundation) under Germany's Excellence Strategy EXC-2111-390814868 and TRR 80. H.-K. J. is funded by the European Research Council (ERC) under the European Unions Horizon 2020 research and innovation program (grant agreement No. 771537). W. M. H. N. and J. K. acknowledge the support from the Royal Society via a Newton International Fellowship through project NIF\R1\181696.

- 
- [1] C. Broholm, R. J. Cava, S. A. Kivelson, D. G. Nocera, M. R. Norman, and T. Senthil, *Science* **367** (2020), 10.1126/science.aay0668.
- [2] J. Knolle and R. Moessner, *Annual Review of Condensed Matter Physics* **10**, 451 (2019).
- [3] Y. Zhou, K. Kanoda, and T.-K. Ng, *Rev. Mod. Phys.* **89**, 025003 (2017).
- [4] L. Savary and L. Balents, *Reports on Progress in Physics* **80**, 016502 (2016).
- [5] A. Kitaev, *Annals of Physics* **321**, 2 (2006), January Special Issue.
- [6] C. Nayak, S. H. Simon, A. Stern, M. Freedman, and S. Das Sarma, *Rev. Mod. Phys.* **80**, 1083 (2008).
- [7] G. Jackeli and G. Khaliullin, *Physical Review Letters* **102**, 017205 (2009).
- [8] J. c. v. Chaloupka, G. Jackeli, and G. Khaliullin, *Phys. Rev. Lett.* **105**, 027204 (2010).
- [9] J. G. Rau, E. K.-H. Lee, and H.-Y. Kee, *Annual Review of Condensed Matter Physics* **7**, 195 (2016).
- [10] S. Trebst, "Kitaev materials," (2017), arXiv:1701.07056 [cond-mat.str-el].
- [11] M. Hermanns, I. Kimchi, and J. Knolle, *Annual Review of Condensed Matter Physics* **9**, 17 (2018).
- [12] H. Takagi, T. Takayama, G. Jackeli, G. Khaliullin, and S. E. Nagler, *Nature Reviews Physics* **1**, 264 (2019).
- [13] K. W. Plumb, J. P. Clancy, L. J. Sandilands, V. V. Shankar, Y. F. Hu, K. S. Burch, H.-Y. Kee, and Y.-J. Kim, *Phys. Rev. B* **90**, 041112 (2014).
- [14] L. J. Sandilands, Y. Tian, K. W. Plumb, Y.-J. Kim, and K. S. Burch, *Phys. Rev. Lett.* **114**, 147201 (2015).
- [15] A. Banerjee, C. Bridges, J.-Q. Yan, A. Aczel, L. Li, M. Stone, G. Granroth, M. Lumsden, Y. Yiu, J. Knolle, *et al.*, *Nature materials* **15**, 733 (2016).
- [16] S.-H. Do, S.-Y. Park, J. Yoshitake, J. Nasu, Y. Motome, Y. S. Kwon, D. Adroja, D. Voneshen, K. Kim, T.-H. Jang, *et al.*, *Nature Physics* **13**, 1079 (2017).
- [17] S.-H. Baek, S.-H. Do, K.-Y. Choi, Y. S. Kwon, A. U. B. Wolter, S. Nishimoto, J. van den Brink, and B. Büchner, *Phys. Rev. Lett.* **119**, 037201 (2017).
- [18] J. Zheng, K. Ran, T. Li, J. Wang, P. Wang, B. Liu, Z.-X. Liu, B. Normand, J. Wen, and W. Yu, *Phys. Rev. Lett.* **119**, 227208 (2017).
- [19] G. Cao, T. F. Qi, L. Li, J. Terzic, V. S. Cao, S. J. Yuan, M. Tovar, G. Murthy, and R. K. Kaul, *Phys. Rev. B* **88**, 220414 (2013).
- [20] S. Manni, S. Choi, I. I. Mazin, R. Coldea, M. Altmeyer, H. O. Jeschke, R. Valentí, and P. Gegenwart, *Phys. Rev. B* **89**, 245113 (2014).
- [21] J. c. v. Chaloupka, G. Jackeli, and G. Khaliullin, *Phys. Rev. Lett.* **110**, 097204 (2013).
- [22] Y. Yamaji, T. Suzuki, T. Yamada, S.-i. Suga, N. Kawashima, and M. Imada, *Phys. Rev. B* **93**, 174425 (2016).
- [23] P. P. Stavropoulos, X. Liu, and H.-Y. Kee, *Phys. Rev. Research* **3**, 013216 (2021).
- [24] C. Xu, J. Feng, H. Xiang, and L. Bellaiche, *npj Computational Materials* **4** (2018), 10.1038/s41524-018-0115-6.
- [25] C. Xu, J. Feng, M. Kawamura, Y. Yamaji, Y. Nahas, S. Prokhorenko, Y. Qi, H. Xiang, and L. Bellaiche, *Phys. Rev. Lett.* **124**, 087205 (2020).
- [26] H. Liu and G. Khaliullin, *Phys. Rev. B* **97**, 014407 (2018).
- [27] R. Sano, Y. Kato, and Y. Motome, *Phys. Rev. B* **97**, 014408 (2018).
- [28] H. Liu, J. c. v. Chaloupka, and G. Khaliullin, *Phys. Rev. Lett.* **125**, 047201 (2020).
- [29] G. Baskaran, S. Mandal, and R. Shankar, *Phys. Rev. Lett.* **98**, 247201 (2007).
- [30] G. Baskaran, D. Sen, and R. Shankar, *Phys. Rev. B* **78**, 115116 (2008).
- [31] S. Chandra, K. Ramola, and D. Dhar, *Phys. Rev. E* **82**, 031113 (2010).
- [32] J. Oitmaa, A. Koga, and R. R. P. Singh, *Phys. Rev. B* **98**, 214404 (2018).
- [33] A. Koga, H. Tomishige, and J. Nasu, *Journal of the Physical Society of Japan* **87**, 063703 (2018).
- [34] I. Rousochatzakis, Y. Sizyuk, and N. B. Perkins, *Nature communications* **9**, 1 (2018).
- [35] X.-Y. Dong and D. N. Sheng, *Phys. Rev. B* **102**, 121102 (2020).
- [36] H.-Y. Lee, N. Kawashima, and Y. B. Kim, *Phys. Rev. Research* **2**, 033318 (2020).
- [37] S. R. White, *Physical review letters* **69**, 2863 (1992).
- [38] S. R. White, *Physical Review B* **48**, 10345 (1993).
- [39] F. Wang and A. Vishwanath, *Phys. Rev. B* **80**, 064413 (2009).
- [40] W. M. H. Natori, E. C. Andrade, E. Miranda, and R. G. Pereira, *Phys. Rev. Lett.* **117**, 017204 (2016).
- [41] W. M. H. Natori, M. Daghofer, and R. G. Pereira, *Phys. Rev. B* **96**, 125109 (2017).
- [42] W. M. H. Natori, E. C. Andrade, and R. G. Pereira, *Phys. Rev.*

- B 98**, 195113 (2018).
- [43] H. Yao, S.-C. Zhang, and S. A. Kivelson, *Phys. Rev. Lett.* **102**, 217202 (2009).
- [44] V. Chua, H. Yao, and G. A. Fiete, *Physical Review B* **83**, 180412 (2011).
- [45] H. Yao and D.-H. Lee, *Phys. Rev. Lett.* **107**, 087205 (2011).
- [46] V. S. de Carvalho, H. Freire, E. Miranda, and R. G. Pereira, *Phys. Rev. B* **98**, 155105 (2018).
- [47] S. Chulliparambil, U. F. P. Seifert, M. Vojta, L. Janssen, and H.-H. Tu, *Phys. Rev. B* **102**, 201111 (2020).
- [48] C. S. de Farias, V. S. de Carvalho, E. Miranda, and R. G. Pereira, *Phys. Rev. B* **102**, 075110 (2020).
- [49] U. F. P. Seifert, X.-Y. Dong, S. Chulliparambil, M. Vojta, H.-H. Tu, and L. Janssen, *Phys. Rev. Lett.* **125**, 257202 (2020).
- [50] W. M. H. Natori and J. Knolle, *Phys. Rev. Lett.* **125**, 067201 (2020).
- [51] S. Ray, B. Ihrig, D. Kruti, J. A. Gracey, M. M. Scherer, and L. Janssen, *Phys. Rev. B* **103**, 155160 (2021).
- [52] S. Chulliparambil, L. Janssen, M. Vojta, H.-H. Tu, and U. F. P. Seifert, *Phys. Rev. B* **103**, 075144 (2021).
- [53] An iterative scheme has been employed to find the self-consistent solutions to Eq. (5), where different randomly-generated  $Q$  and  $\Delta$  are selected to initialize the iterations. If multiple inequivalent solutions occurred, we will select the solution with the lowest mean-field ground-state energy.
- [54] F. J. Burnell and C. Nayak, *Phys. Rev. B* **84**, 125125 (2011).
- [55] J. Knolle, S. Bhattacharjee, and R. Moessner, *Phys. Rev. B* **97**, 134432 (2018).
- [56] E. H. Lieb, *Phys. Rev. Lett.* **73**, 2158 (1994).
- [57] H.-K. Jin, H.-H. Tu, and Y. Zhou, *Phys. Rev. B* **101**, 165135 (2020).
- [58] H.-K. Jin, H.-H. Tu, and Y. Zhou, *Phys. Rev. B* **104**, L020409 (2021).
- [59] Y.-H. Wu, L. Wang, and H.-H. Tu, *Phys. Rev. Lett.* **124**, 246401 (2020).
- [60] S.-S. Zhang, G. B. Halász, W. Zhu, and C. D. Batista, “Variational study of the kitaev-heisenberg-gamma model,” (2021), [arXiv:2103.13274 \[cond-mat.str-el\]](https://arxiv.org/abs/2103.13274).